Supporting Information for Freshwater Contributions to Decadal Variability of the Indonesian Throughflow

Shouyi Wang [1,2], Caroline C. Ummenhofer[2], Delia W. Oppo[2], Sujata A. Murty[2,3], Patrick Wagner[4], Claus W. Böning[4], Arne Biastoch[4,5]

[1]MIT-WHOI Joint Program in Oceanography/Applied Ocean Sciences & Engineering, Cambridge and Woods Hole, MA, USA

[2]Woods Hole Oceanographic Institution, Woods Hole, MA, USA

[3]University at Albany, State University of New York, Albany, NY, USA

[4]GEOMAR Helmholtz Centre for Ocean Research Kiel, Kiel, Germany

[5]Kiel University, Kiel, Germany

Contents of this file

Corresponding author: S. Wang, Woods Hole Oceanographic Institution, Woods Hole, MA (syiwang@mit.edu)

Model Validation

Timeseries of volume transport through the Luzon, Sibutu, and Karimata Straits on seasonal, interannual, and decadal timescales is shown and discussed to assess the model's skill in characterizing South China Sea circulation (Figure S1). A detailed comparison between observed Labani mooring velocity measurements and co-located velocities in ORCA025 (Figure S2) is discussed below. Also included are figures which show assessment of the salinity restoring term (Figure S3), the vertical profile of ITF density difference variability in the upper 300m with and without temperature variations (Figure S4), timeseries of the U130m local density gradient compared to the SSH gradient on seasonal, interannual, and decadal timescales (Figure S5), the decomposition of UST into various timescales (Figure S6), the annual mean (1960-2017) U130m velocity field of the ITF study region compared against decadal anomalies(Figure S7), the regional temperature anomalies on various timescales (Figure S8). A comparison of decadal UST to the large-scale pressure gradient and the local pressure gradient is given (Figure S9).

A comparison of volume transport through the Sibutu Passage, Karimata Strait, and the upper 500m of the Luzon Strait (the depth range of shallow inflow; Sun et al., 2023) shows that ORCA025 accurately characterizes the transport variability of the SCS passageways on seasonal to decadal timescales. Specifically, the seasonal variability of the Karimata and Sibutu passages volume transport varies in concert with the upper Luzon Strait inflow (Figure S1a-b). On interannual-decadal timescales however, upper Luzon Strait transport variability is largely proportional to Sibutu Passage variations (Figure S1c-f), with the Karimata Strait varying minimally. This discrepancy in the ocean model

between the two shallow passageways, which agrees well with previous studies of SCS circulation (Gordon et al., 2012; Wei et al., 2016; Jiang et al., 2019), is due to the dominant monsoonal signal in the southern SCS and Java Sea, which minimizes interannual and decadal variations of the Karimata throughflow. Important to note is that while upper Luzon inflow matches well with Sibutu Passage outflow in magnitude, enhanced vertical mixing in the SCS cools and freshens these inflow waters along their path through the SCS (Deng et al., 2018; Wang et al., 2017).

We compare the Makassar Strait velocity profile between 40-630m at the Labani channel between ORCA025 and observations. For all comparisons, we analyze the period where both data types were available (2004-2017) and calculate anomalies the same way. Thus while we have 57 years of ocean model data, only 13 of them were used for this comparison because of the limited observational record. The simulated velocity profile was constructed by averaging the nine gridpoints closest to the Labani mooring location in the model. The average southward velocity profile in the observations exhibits a profile with high surface velocities (maximum values up to 0.6 m/s at $\sim$ 130m) which decrease with depth down to 0.1 m/s at 630m (Figure S2a). The simulated average velocity profile qualitatively resembles the observations with surface intensification, however, the ocean model underestimates the absolute magnitude at all depths (Figure S2a). In the ocean model, southward velocities in the upper 200m only reach a maximum of 0.4 m/s and below 300m depth, velocities decrease to 0 m/s. On seasonal timescales, the upper 200m in both observations and the ocean model exhibit elevated southward velocities during July-September (increase of 0.2 m/s) and reduced values during November-January (decrease

of 0.2 m/s), driven by the seasonal freshwater plug (Figure S2b-c). Below this surface layer at 300-630m, the model skillfully captures the semi-annual Kelvin waves that increase velocities by 0.1 m/s during January-March and June-August and decrease velocities by 0.1 m/s in April-June and October-December (Figure S2b-c). We also compare the velocity anomalies for 1 year following the wintertime peak of ENSO events between ORCA025 and the observations. Following El Niño events, velocities in the upper 300m decrease for 10-11 months by around 0.05 m/s in the observations and 0.03 m/s in ORCA025. In contrast, the 300-630m layer exhibits an increase in southward velocities up to 0.08 m/s in the observations and 0.03 m/s in the model (Figure S2d-e). La Niña events induce an opposite response, with observational velocities increasing up to 0.08 m/s in the upper 300m and decreasing by 0.06 m/s below while simulated velocities elevate by 0.05 m/s and decrease by 0.03 m/s in the upper and lower 300m respectively (Figure S2f-g). Overall, ORCA025 accurately captures the sign and timing of velocity profile changes in response to ENSO albeit with weaker amplitudes than observations.

River runoff, which is an important driver of seasonal ITF transport, is parameterized in ORCA025 as daily freshwater input into the first vertical level at a singular gridbox at the river mouth. The impact of SSS restoring on the tropical Indo-Pacific salinity budget was assessed by comparing the restoring freshwater flux term to the total freshwater flux term (Figure S3). Compared to the total freshwater flux, the restoring flux is much smaller in amplitude (<10% in most regions). In addition, while the total freshwater flux displays the spatial pattern of the Indo-Pacific Intertropical Convergence Zone and exhibits pronounced seasonality (Figure S3b,d,f), the restoring flux does not resemble tropical rainfall

and appears seasonally invariant (Figure S3a,c,e). We therefore conclude that model SSS restoring in ORCA025 does not significantly impact the regional salinity budget for this study.

References

Deng, H., Huang, P., Tanhua, T., Stöven, T., Ke, H., Guo, W., ... Cai, M. (2018). Observations of the Intermediate Water Exchange Between the South China Sea and the Pacific Ocean Deduced From Transient Tracer Measurements. *Journal of Geophysical Research: Oceans*, *123*(10), 7495–7510. Retrieved 2023-07-04, from https://onlinelibrary.wiley.com/doi/abs/10.1029/2018JC014103 (_eprint: https://onlinelibrary.wiley.com/doi/pdf/10.1029/2018JC014103) doi: 10.1029/2018JC014103

Gordon, A. L., Huber, B. A., Metzger, E. J., Susanto, R. D., Hurlburt, H. E., & Adi, T. R. (2012, June). South China Sea throughflow impact on the Indonesian throughflow. *Geophysical Research Letters*, *39*(11), n/a–n/a. Retrieved 2022-08-02, from http://doi.wiley.com/10.1029/2012GL052021 doi: 10.1029/2012GL052021

Jiang, G., Wei, J., Malanotte-Rizzoli, P., Li, M., & Gordon, A. L. (2019, December). Seasonal and Interannual Variability of the Subsurface Velocity Profile of the Indonesian Throughflow at Makassar Strait. *Journal of Geophysical Research: Oceans*, *124*(12), 9644–9657. Retrieved 2022-08-02, from https://onlinelibrary.wiley.com/doi/10.1029/2018JC014884 doi: 10.1029/2018JC014884

Sun, Z., Zhang, Z., Huang, R. X., Gan, J., Zhou, C., Zhao, W., & Tian, J. (2023). Novel Insights Into the Zonal Flow and Transport in the Luzon Strait Based on Long-Term Mooring Observations. *Journal of Geophysical Research: Oceans*, *128*(3), e2022JC019017. Retrieved 2023-07-04, from https://onlinelibrary.wiley.com/doi/abs/10.1029/2022JC019017 (_eprint: https://onlinelibrary.wiley.com/doi/pdf/10.1029/2022JC019017) doi: 10.1029/

2022JC019017

Wang, X., Liu, Z., & Peng, S. (2017, February). Impact of Tidal Mixing on Water Mass Transformation and Circulation in the South China Sea. *Journal of Physical Oceanography*, *47*(2), 419–432. Retrieved 2023-06-29, from https://journals.ametsoc.org/view/journals/phoc/47/2/jpo-d-16-0171.1.xml (Publisher: American Meteorological Society Section: Journal of Physical Oceanography) doi: 10.1175/JPO-D-16-0171.1

Wei, J., Li, M. T., Malanotte-Rizzoli, P., Gordon, A. L., & Wang, D. X. (2016, October). Opposite Variability of Indonesian Throughflow and South China Sea Throughflow in the Sulawesi Sea. *Journal of Physical Oceanography*, *46*(10), 3165–3180. Retrieved 2023-05-01, from https://journals.ametsoc.org/view/journals/phoc/46/10/jpo-d-16-0132.1.xml (Publisher: American Meteorological Society Section: Journal of Physical Oceanography) doi: 10.1175/JPO-D-16-0132.1

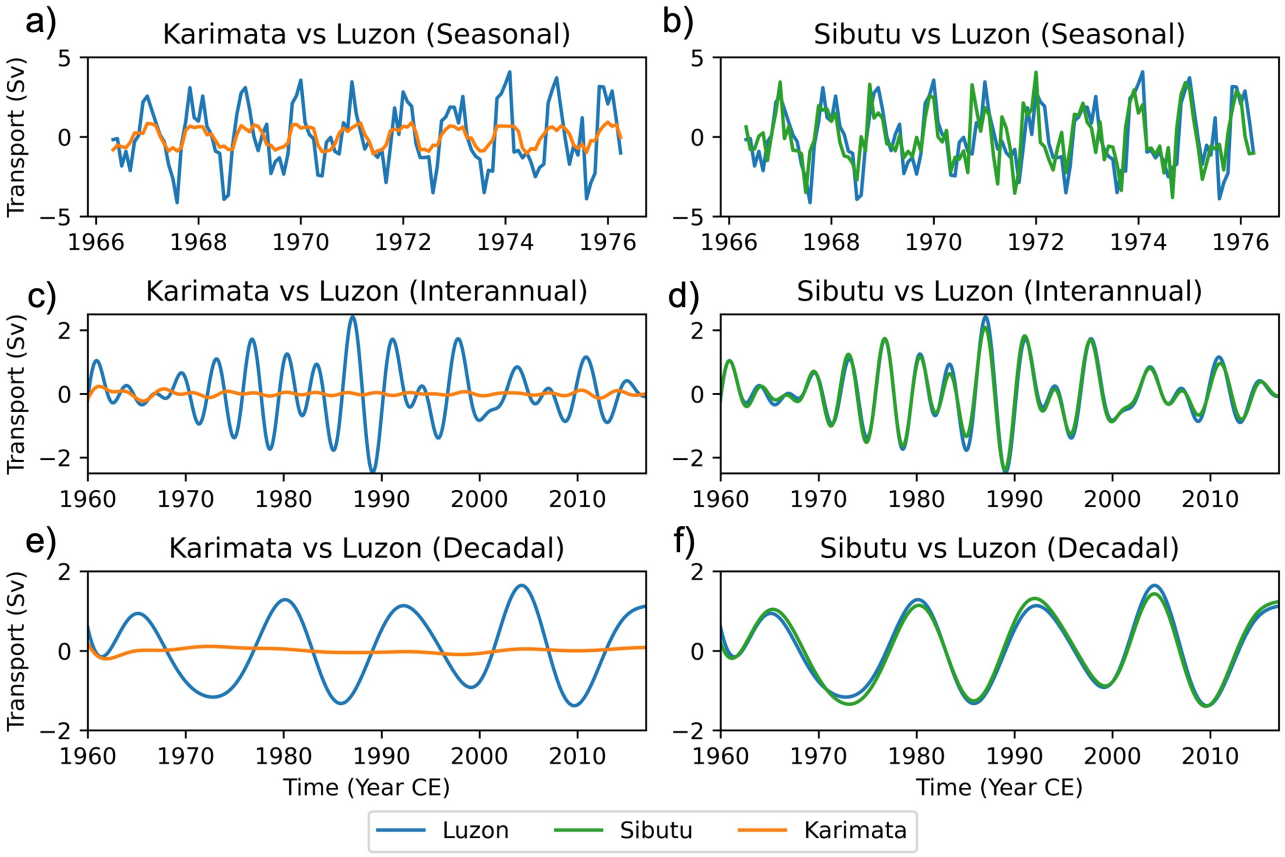

Figure S1. Comparison of simulated volume transport variability through the Karimata Strait (integrated from surface to bottom, 45m sill depth) and the upper 230m of the Luzon Strait on seasonal (**a**), interannual (**c**), and decadal (**e**) timescales. Sibutu Passage (integrated from surface to bottom, 230m sill depth) comparison to upper 500m Luzon Strait on seasonal (**b**), interannual (**d**), and decadal (**f**) timescales is also shown. Transects for volume transport calculation are based on red sections in Figure 1b.

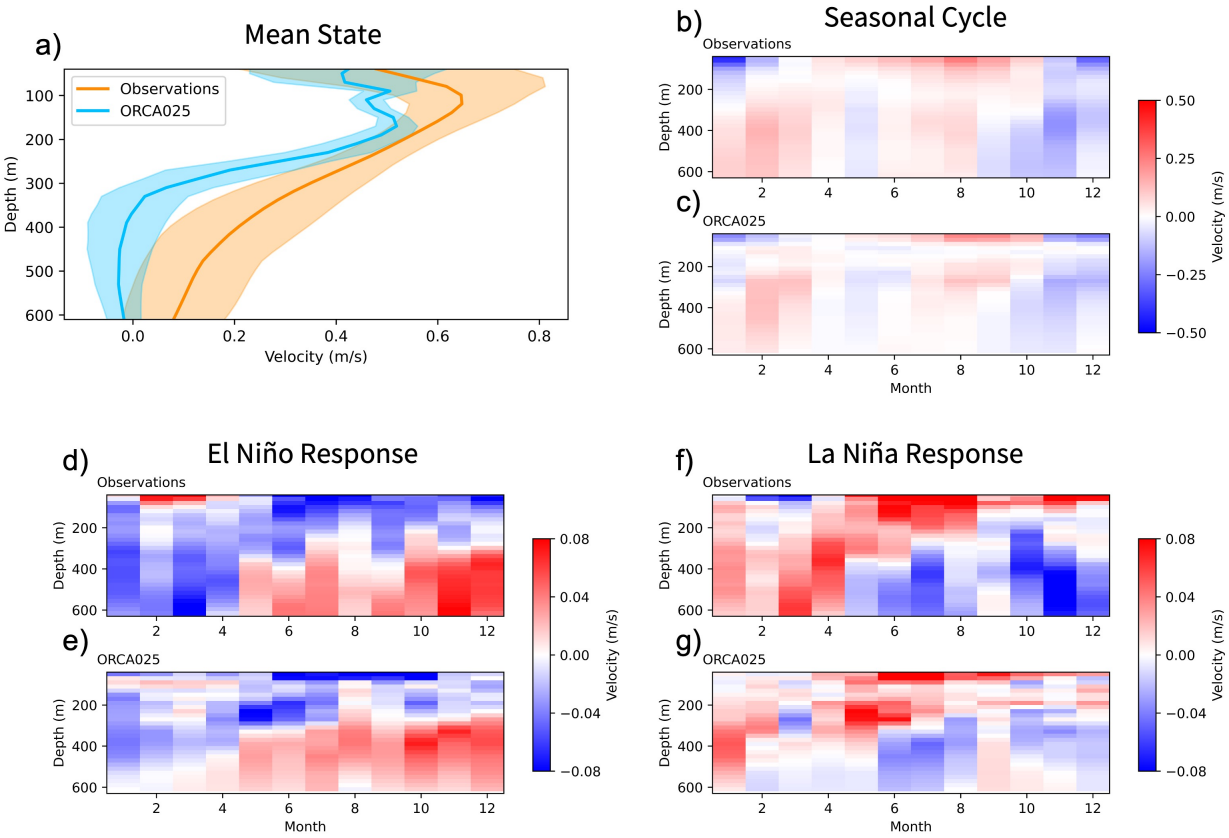

Figure S2. Velocity profile (40-630m) in observations (orange) and ORCA025 (blue) at the Labani mooring location, mean southward velocity in thick colored line and 1 standard deviation spread in colored shading **(a)**. The seasonal cycle of southward velocity anomalous from the long-term annual mean (2004-2017) in observations **(b)** and ORCA025 **(c)**. The evolution of the velocity profile anomalies in the year following the peak boreal winter ENSO event in observations **(d,f)** and ORCA025 **(e,g)** for El Niño **(d,e)** and La Niña **(f,g)**. ENSO years were identified when the 3-month running average of the Niño3.4 Index during DJF exceeded 0.5^{o}C. Based on this threshold, the available mooring data (13 years) contained 4 El Niño years (2004/2005, 2006/2007, 2009/2010, 2014/2015) and 4 La Niña years (2005/2006, 2007/2008, 2008/2009, 2010/2011).

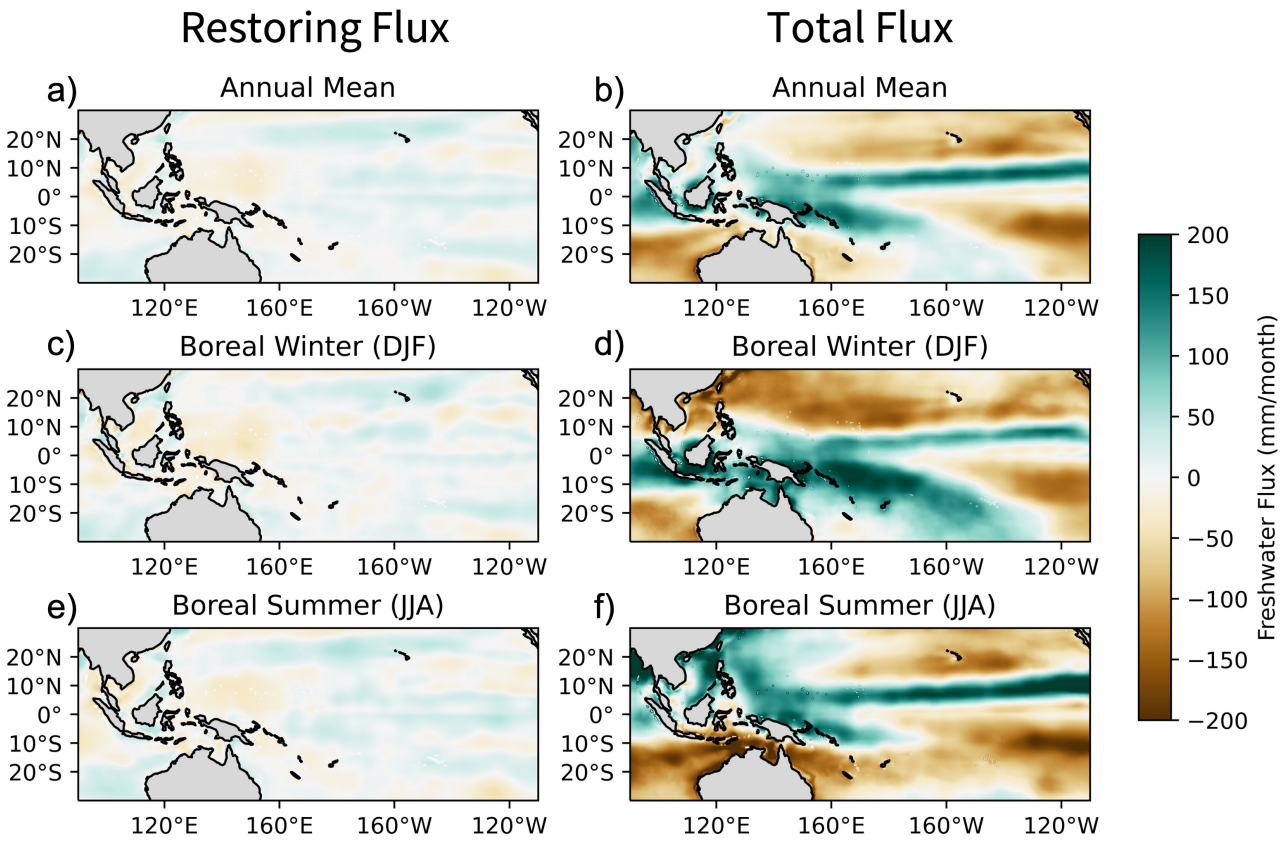

Figure S3. Mean (1958-2017) surface freshwater flux in ORCA025 in the tropical Indo-Pacific due to model SSS restoring (**a,c,e**) versus total freshwater flux into the ocean model (**b,d,f**) for all months of the year (**a,b**), DJF months only (**c,d**), and JJA months only (**e,f**).

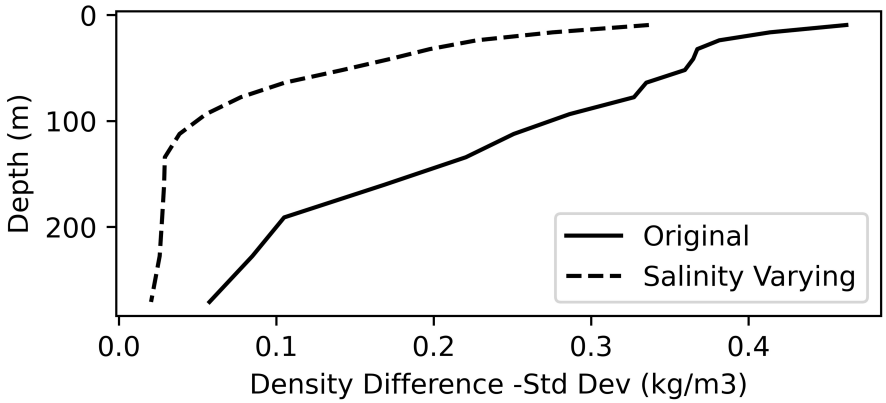

Figure S4. Annual mean (1958-2017) standard deviation of density difference between Makassar Strait (Figure 1b, orange box) and Mindanao-Sulawesi Passage (Figure 1b, purple box) as a function of depth for the upper 300m. Density difference was calculated with salinity and temperature varying (solid black line) and with temperature held constant (dashed line)

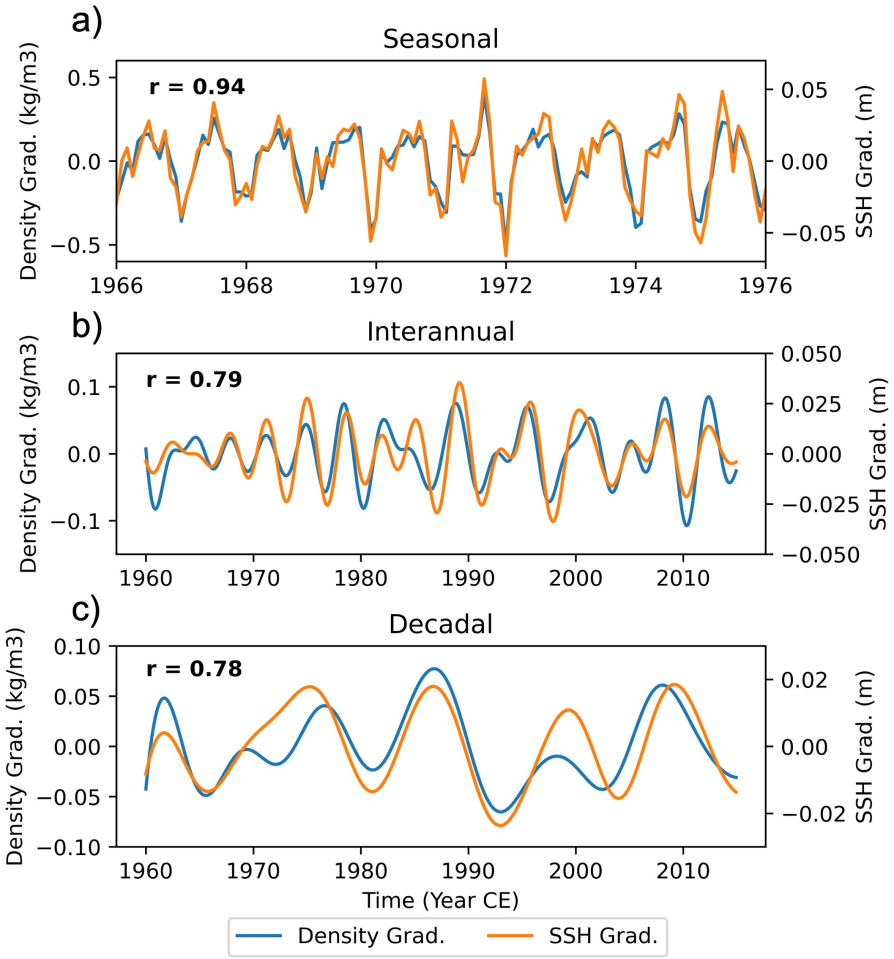

Figure S5. Timeseries of U130m average density gradient (blue) and sea surface height gradient (orange) anomalies between the Makassar Strait and the Mindanao-Sulawesi Massage (using Figure 1b boxes) on seasonal (**a**), interannual (**b**), and decadal (**c**) timescales. Pearson correlation coefficients on each respective timescale are also shown, all of which are significant at $p<0.001$.

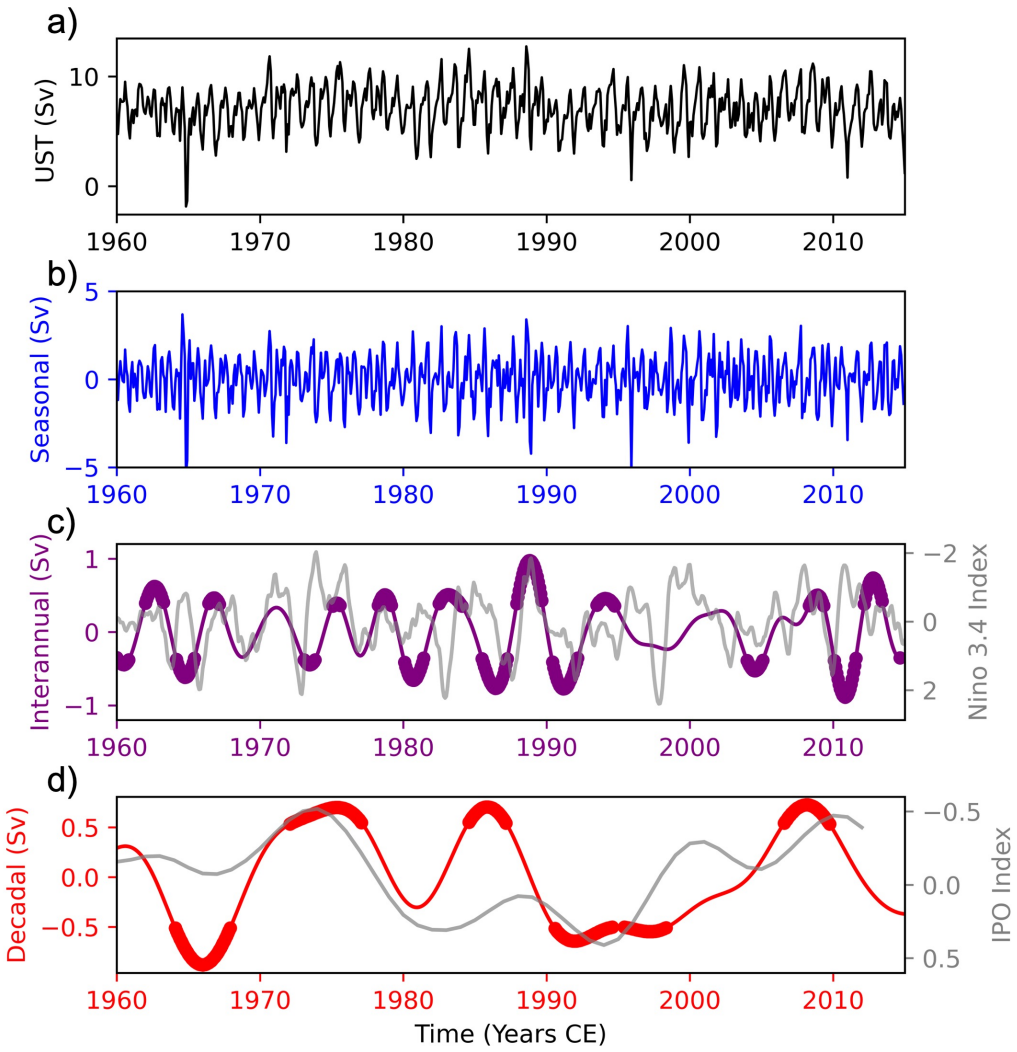

Figure S6. U130m Makassar Strait southward transport **(a)** and its decomposition into variability on seasonal **(c)**, interannual **(b)**, and decadal **(d)** timescales. Periods of low and high UST are indicated by thick dots for interannual and decadal components. Niño 3.4 Index and IPO Index are inverted and plotted in gray on the interannual and decadal components respectively **(b,d)** (See Methods 2.4 for details).

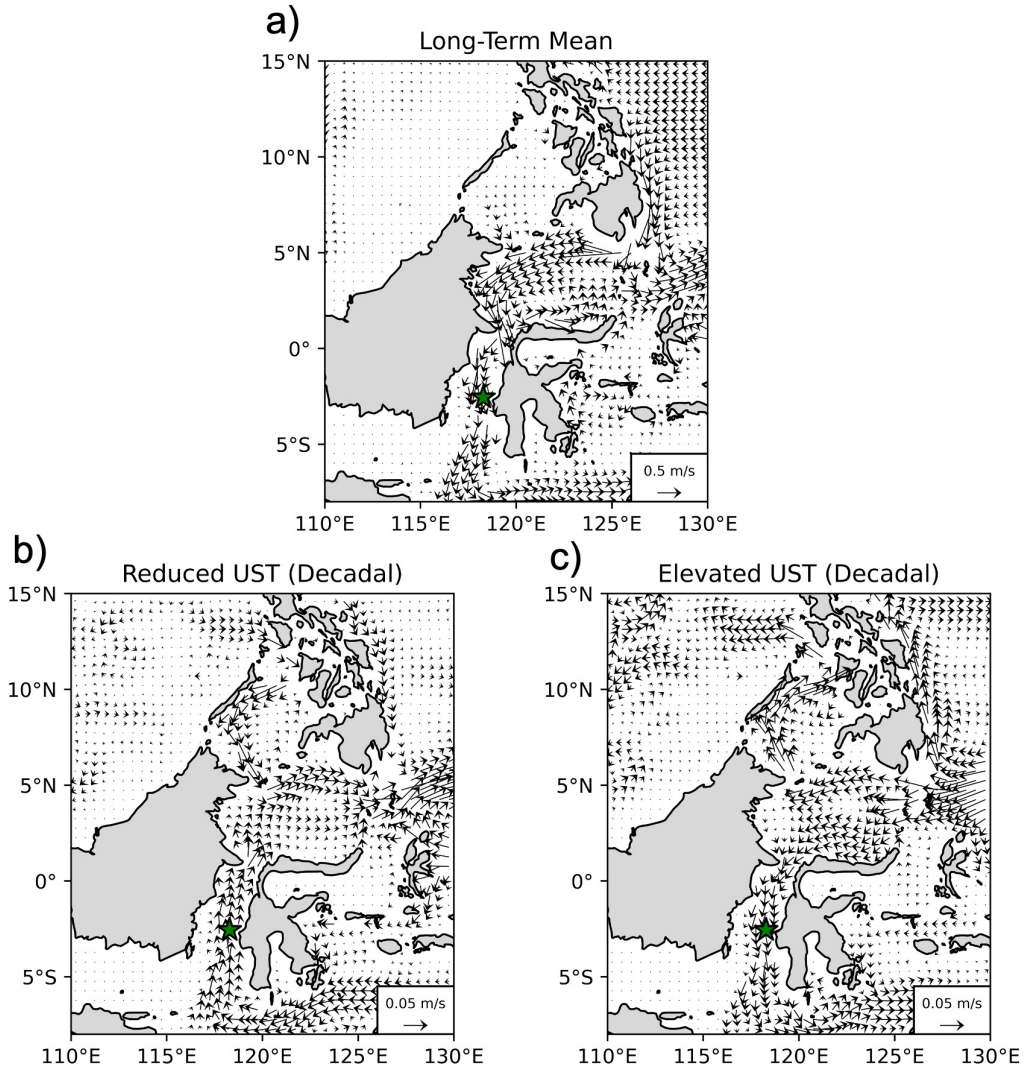

Figure S7. Annual mean (1960-2017) simulated U130m velocity for the ITF study region **(a)**. U130m velocity anomalies during reduced **(b)** and elevated UST **(c)** periods on decadal timescales, identical to vectors in Figure 3a-b. Note that the reference vector for the mean flow is an order of magnitude greater than the anomaly vector reference vector (0.5 m/s vs 0.05 m/s), highlighting that southward flow through Makassar Strait is persistent across identified reduced UST periods. The Labani mooring location is indicated (green star).

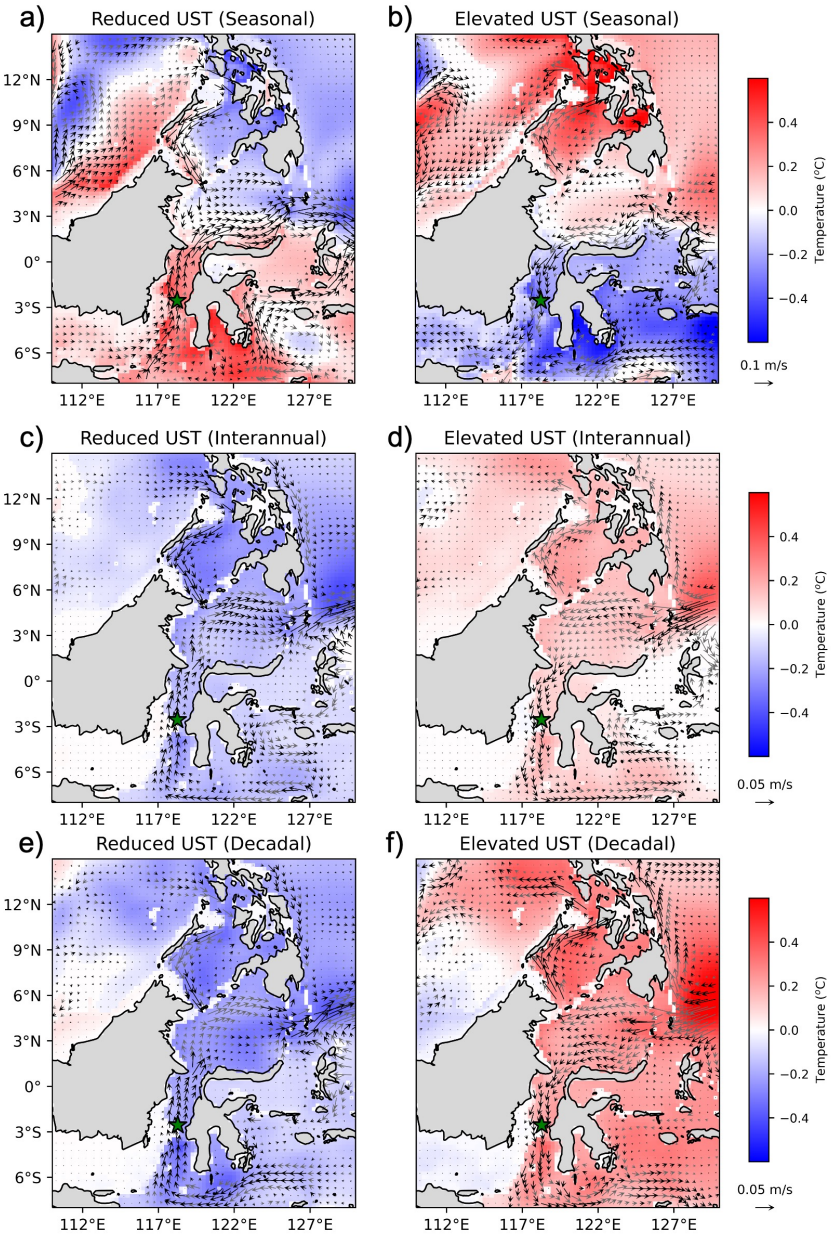

Figure S8. Composite maps of U130m average temperature and velocity anomalies during periods of low and high UST on seasonal (**a,b**), interannual (**c,d**), and decadal (**e,f**) timescales. Only temperature anomalies significant at the 90% level, determined from Monte-Carlo resampling, are shown. Both velocity anomalies significant at the 90% level (black vectors) and those below (grey vectors) are shown. Labani mooring location is indicated (green star).

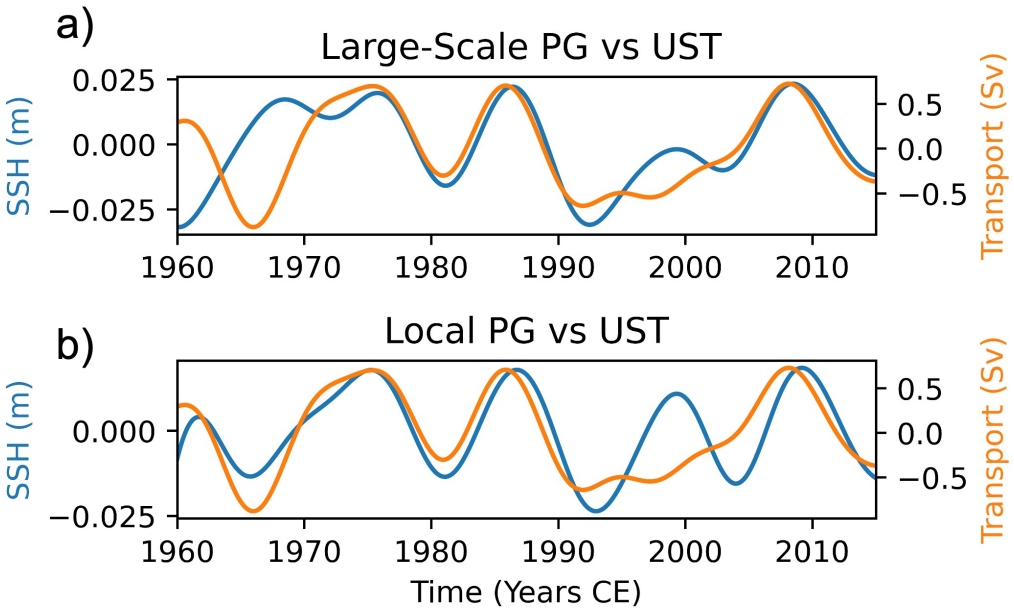

Figure S9. Timeseries of the decadal component of the inter-basin SSH difference (Large-Scale PG) vs decadal UST (**a**). Timeseries of the decadal component of the local SSH difference (local PG) vs decadal UST (**b**). The large-scale pressure gradient was defined as difference in average SSH between the western Pacific (125^{o}E to 135^{o}E and 0^{o}N to 10^{o}N) and the eastern Indian Ocean (112^{o}E to 122^{o}E and 18.5^{o}S to 9^{o}S). The local PG was defined as the average SSH difference between the Makassar Strait (Figure 1b orange box) and the Mindanao-Sulawesi Passage (Figure 1b purple box).